

Biomedical Engineering

Chapter 1

Arginine Substituted Phthalocyanine with Positive Charge in Wide pH Range as Efficient Photosensitizer for Photodynamic Therapy

Kang Sun*

**Institute of Chemical Industry of Forest Products, Key Lab of Biomass Energy and Material, Jiangsu Province, National Engineering Lab. For Biomass Chemical Utilization, Key and Open Lab. of Forest Chemical Engineering, SFA, Chinese Academy of Forestry, No. 16, Suojin 5th Village, Nanjing 210042, China.*

Email: sunkang0226@163.com

Abstract

Drugs with positive charge usually have good water solubility, enhanced cellular uptake efficiency and activity. However, the preparation of quaternized drugs need potentially dangerous agents, while protonated cationic drugs are easily deprotonated in alkaline solutions. Arginine can be positively charged in a wide range of pH. Thus, two phthalocyanine-arginine conjugates (ArgEZnPc and ArgZnPc) were reported in this paper. They can be positively charged in the range of pH 5 to 9. Besides, the photochemical and photobiological properties, subcellular localization, anticancer activities of the them were also carried out. The results show that ArgEZnPc has high water solubility, excellent singlet oxygen and reactive oxygen species generation efficiency, can preferentially localize in the lysosomes of HeLa cells. The above results lead to a high in vitro anticancer activity of ArgEZnPc and make it a promising photosensitizer for photodynamic therapy.

Key words: Photodynamic therapy; Photosensitizer; Phthalocyanine; Arginine

1. Introduction

Photodynamic therapy (PDT), which uses non-toxic photosensitizers (PSs) and harmless visible light to produce highly cytotoxic reactive oxygen species (ROSs) and destroy tumors in the presence of oxygen is an emerging approach for cancer treatment [1-3]. Since the properties of PSs including water solubility, aggregation, cellular uptake and ROSs generation efficiency is the key factor that influence the final therapeutic outcome of PDT, most research efforts have been devoted to optimize the photochemical and photobiological characteristics of PSs [4-8]. Charge is closely related to the above properties of PSs [9]. In general, positively charged molecules have enhanced water solubility, cellular uptake efficiency and anticancer activity. [10-12]. Hence, various PSs with positive charge have been prepared and been reported to have better therapeutic effect [13-17]. For example, Makhseed et al., Zimcik et al., and Huang et al. have reported several positively charged cationic phthalocyanines (Pcs) as water soluble, non-aggregated and efficient PSs [13-15]. Ju et al. and O'Shea et al. have reported amine containing PSs that can switch their charge from neutral to positive to get high singlet oxygen ($^1\text{O}_2$) quantum yields [16,17].

To prepare positively charged PSs, two common methods are usually used: quaternization and protonation of aliphatic or aromatic nitrogen atoms [18,19]. In preparing quaternized PSs, methylating agents are always required. Since the methylating agents are potentially dangerous as they are likely to methylate DNA, they must be used with care [19]. Besides, extra works are needed to purify the quaternized PSs, which also increases the work load. In contrast, there is no need of toxic methylating agents for preparing protonated PSs. Accordingly, the prepare processes are simple. Moreover, the photochemical activities of protonated PSs may be similar, even superior, to the quaternized ones [18]. However, the protonated PSs are easily deprotonated in alkaline circumstance such as normal physiological (pH ca.7.4), which limits their practical application [18,20,21].

Arginine is the building blocks of cytoplasm and nucleic acid protein [22]. It is unique among the amino acids as its guanidine group has exceptionally high basicity in aqueous solution ($\text{pK}_a=13.5$), which makes it positively charged in a wide range of pH [23-25]. What's more, guanidine group or arginine substituted drugs always show enhanced cellular uptake efficiency, tumor targeting ability and anticancer activity [26-28]. These enhanced properties are related to the strong basicity of guanidine [29]. Pcs are a versatile class of functional dyes, which are the most efficient and common used PSs in PDT due to their strong absorption in visible range, high efficiency in ROSs generation, low dark toxicity and efficient phototoxicity to cancer cells [30,31].

Based on the above conceptions, two arginine substituted zinc Pcs were prepared [32]. In addition, the charge properties of them in a wide range of pH values was studied. Their

photobiological, photochemical properties, subcellular localization and in vitro anticancer activities for PDT use also have been studied.

2. Results and Discussion

2.1. Synthesis

The structures of ArgZnPc and ArgEZnPc are shown in **Figure 1**. The synthesis and characterization of the two Pcs were prepared as follows [32]. Firstly, the tetra-carboxyl benzyloxyl phthalocyaninato zinc (CbZnPc) was prepared by annelation reactions. After then, the ArgZnPc and ArgEZnPc were both synthesized through amidation reaction by using N-(3-Dimethylamino-propyl)-N'-ethylcarbodiimide hydrochloride (EDC•HCl) and 1-Hydroxybenzotriazole (HOBt) as the catalyst.

2.2. Charge properties of ArgZnPc and ArgEZnPc at different pHs

As mentioned above, though protonated drugs are easily deprotonated in alkaline solutions, [18,20,21] arginine substituted ones can be positively charged in a wide range of pH due to the guanidine group [23-25]. To confirm this, the charge properties of ArgZnPc and ArgEZnPc at various pH levels were measured. Since the two ZnPcs both have good water solubility, their zeta potentials were measured in water of different pHs. As shown in **Figure 2**, both ArgZnPc and ArgEZnPc are positively charged at the pH range of 5-9, which is in accord with the previous reports, proves the correctness of our concept. In addition, from **Figure 2** it also can be seen that both the zeta potentials of ArgZnPc and ArgEZnPc decreased as the pH values increase, but the decrease was small in the pH range of 5-7, which indicates that the two Pcs are fully protonated at this pH range. In contrast, the zeta potentials of ArgZnPc decreased sharply when the pH increase from 7 to 9, which indicates the deprotonation of ArgZnPc. Even so, at the experimental pH range, ArgZnPc was always positively charged. The zeta potential of ArgEZnPc also decreased as the pH increase from 7 to 9, while the decrease was smaller than the decrease of ArgZnPc. This may be contributed to the higher basicity of ArgEZnPc, which makes it more difficult to be deprotonated.

2.3. Aggregation and electronic absorption properties

The aggregation and electronic absorption properties of ArgEZnPc and ArgZnPc were studied in distilled water. As shown in **Figure 3A**, Both the two ZnPcs gave typical absorption spectra of aggregated Pcs, showing the B band at about 340 nm, Q band at 630-640 nm [33]. The reason for this may be that due to the charged substituents of the two Pcs are mostly freely pending, the electrostatic repulsion force can not prevent aggregation of them [11,13]. Moreover, the significant differences in the Q-band absorptions indicate that the macrocyclic π system is perturbed by the peripheral substituents though the substituents of ArgZnPc and

ArgEZnPc are very similar. **Figure 3B** and **3C** show the electronic absorption of ArgZnPc and ArgEZnPc in water at various concentrations. The Q band absorption of them follows the Lambert-Beer law strictly, which indicate that the aggregation form of them may have little change as the concentration increase.

Dynamic-light-scattering experiments (DLS) are always used to demonstrate the aggregation properties of the examined compounds[34]. Thus, to further studied the aggregation properties of ArgEZnPc and ArgZnPc, DLS experiments were done subsequently. **Figure 3D** and **3E** show that ArgEZnPc has an average diameter of about 91.77 ± 3.21 nm, while ArgZnPc has an average diameter of about 144.6 ± 4.68 nm. The above results suggest that ArgEZnPc has less aggregation potency than ArgZnPc. Besides, it should note that a diameter of about 1.84 ± 0.10 nm can also be observed in **Figure 3E** for ArgZnPc, which can be attributed to the monomer of it in water. This phenomenon is consistent with the electronic absorption of ArgZnPc (**Figure 3C**), in which there is also a small amount of monomer absorption band at about 680 nm.

Upon excitation at 610 nm, both the two ZnPcs showed very weak fluorescence emission (data not shown). Since aggregates are well known for their low fluorescence, the above fluorescence emission results can be attributed to the aggregation-induced fluorescence quenching [35].

2.4. Photosensitizing properties

It is well known that ROS is responsible for the tumor cells damage, and $^1\text{O}_2$ has been proven to be the main cytotoxic agent of PDT to cause biological effects. Thus, to evaluate the photosensitizing efficiency of ArgZnPc and ArgEZnPc, the $^1\text{O}_2$ generation abilities of them were measured by a steady-state method using ADPA as the scavenger.

As shown in **Figure 4A**, the absorbance intensity of ADPA at 378 nm was gradually decreased with the prolonged light exposure time after irradiation of the mixture of ArgEZnPc and ADPA which suggests the production of $^1\text{O}_2$. Similar phenomenon can be detected after the irradiation of the mixture of ArgZnPc and ADPA, but the absorbance intensity decreasing rate of the ADPA is different (**Figure 4B**). As shown in **Figure 4C**, in water, the $^1\text{O}_2$ generation abilities of ArgZnPc and ArgEZnPc are 4.34×10^{-4} (0.983) and 2.68×10^{-3} (R=0.981) respectively, at the same conditions. The results show that the $^1\text{O}_2$ generation ability of ArgEZnPc is higher than ArgZnPc, though both of them are highly aggregated in water. This may be due to that the zeta potential of ArgEZnPc is higher than ArgZnPc, which results in the higher $^1\text{O}_2$ generation ability [36].

Because photostability of PS is important for their applications as photocatalysts, [33,37] we studied the photobleaching properties of the two ZnPcs by recording the decrease in the

intensity of the spectra (main Q band, **Figure 5A** and **Figure 5B**). After 180 s irradiations, the Q band absorbance intensity of ArgEZnPc and ArgZnPc only show negligible decrease, which indicates the good photostability of them (**Figure 5C**).

2.5. Cellular uptake

UV-Vis spectrophotometry was used to study the uptakes of ArgEZnPc and ArgZnPc by HeLa cells. Figure 6 shows the time-dependent cellular uptake percentage of the two PSs. It can be seen that the uptakes of ArgEZnPc and ArgZnPc by HeLa cells increase gradually with the increase of time. After incubation for 24 h, the cellular uptake of ArgEZnPc is significantly higher than ArgZnPc, which is as high as 96%. This result may be again attributed to the carried charge of the two PSs. It is well known that mammalian cell membranes are slightly negatively charged, [38] thus positively charged ArgEZnPc and ArgZnPc can be attracted by HeLa cells via electrostatic interactions, and then internalized through endocytosis. ArgEZnPc carries more positive charges, thus shows higher cellular uptake extent compared to ArgZnPc. Moreover, guanidine groups of ArgEZnPc can interact with cell membrane phospholipids strongly through hydrogen bonds [39], which may also enhance its cellular uptake efficiency. In contrast, guanidine groups of ArgZnPc may prefer to form inner salt with carboxyl groups through hydrogen bonds, therefore cannot interact with cell membrane phospholipids [40,41]. This may be another reason for the low cellular uptake extent of ArgZnPc.

2.6. Intracellular ROSs generation efficiency

In order to evaluate the photosensitizing efficiency of ArgZnPc and ArgEZnPc at cell levels, the intracellular ROSs generation efficiency of them were studied [42]. The intracellular fluorescence of control cells is weak and negligible, which may be the oxygen metabolites (**Figure 7A**). ArgZnPc treated cells show enhanced intracellular fluorescence after light irradiation, which indicates the production of ROSs (**Figure 7B**). The intracellular fluorescence of ArgEZnPc treated cells are the strongest (**Figure 7C**), indicating its effective ROSs generation ability.

As shown in **Figure 8**, the ROSs generation efficiency is expressed as the ratio between intracellular fluorescence intensity. It was found that ArgEZnPc is a good intracellular ROSs generator, with the intracellular fluorescence intensity are about 2.3-fold higher than the fluorescence intensity of ArgZnPc treated cells. This result is generally in good agreement with the results from the $^1\text{O}_2$ generation and cellular uptake studies, which also suggest the better in vitro anticancer activity of ArgEZnPc compared to ArgZnPc.

2.7. Cell morphology

The anticancer activities of ArgEZnPc and ArgZnPc were firstly studied by observing

the cell morphology changes using inverted microscope. It has been reported that the cell morphology will change after PDT, and the anticancer activity of a drug is proportional to the number of cells whose morphology have changed [43]. As shown in **Figure 9A**, the cell morphology of control cells did not have obvious change after irradiation, which indicate that the single light irradiation cannot damage cells. In contrast, after treatment with ArgEZnPc, ArgZnPc and light irradiation at the same time, the HeLa cells changed significantly, characterizing as cell shrinkage and cell scatter, membrane deformation, which indicated the damage of cancer cells by photodynamic actions (**Figure 9B** and **Figure 9C**). Besides, cells treated with ArgEZnPc showed more morphological changes compared to the cells treated with ArgZnPc. This result indicates that ArgEZnPc would show good photocytotoxicity to HeLa cells.

2.8. Hoechst 33342 staining

PDT process will damage tumor cells and induce DNA destruction in nuclear of cancer cells [43]. Thus, the photodynamic activities of PSs also can be judged from the nuclear morphology changes of cells after PDT. To study the PDT induced cancer cell nuclear damage, the cells were stained with Hoechst 33342. The chromatin fluorescence of ArgZnPc treated cells stained dimly and occupied the majority of the cell, which is similar to the control cells (**Figure 10A** and **Figure 10B**). The result demonstrates that ArgZnPc may have low photocytotoxicity to HeLa cells. On the contrary, the nuclear morphology of ArgEZnPc treated cells changed significantly after irradiation, which is characterized as chromatin shrinkage, condensation, and fragmentation. In addition, the chromatin fluorescence intensity is also enhanced. The above phenomenon indicated the chromatin damage.

2.9. Subcellular localization

The subcellular localization of PSs can also determine the outcome of PDT [44,45]. Thus, the localization of ArgZnPc and ArgEZnPc were investigated using a co-location experiments. As shown in Figure 11, the Lyso-Tracker caused fluorescence can superimpose with the fluorescence caused by ArgEZnPc. The similar fluorescence line of ArgEZnPc and Lyso-Tracker traced along with the white arrow in **Figure 11B** also confirms that ArgEZnPc can target the lysosomes of HeLa cells. Though the intracellular fluorescence of ArgZnPc is weak, the in situ fluorescence analysis results also show that it is located in lysosome (**Figure 11B**). In contrast, the fluorescence images of the two ZnPcs could not be merged with the Nu-Tracker, which indicates that they are not localized in nucleus.

2.10. *In vitro* anticancer activity

The photodynamic activity of the two ZnPcs toward HeLa cells was studied using MTT assay [46]. As the positively charged drugs often have more toxicity to normal cells than drugs

with negative and neutral charges, the dose-dependent cytotoxicity of ArgEZnPc and ArgZnPc were studied in the first. As shown in **Figure 12**, in the range of experimental concentrations, both of them are essentially noncytotoxic in the absence of light. However, upon irradiation with 665 nm LED light for 5 min, ArgEZnPc exhibits high cytotoxicity with a cell survival percentage of approximately 13.8% (**Figure 13**). This result is in accord with the previous experimental results, which indicates that ArgEZnPc is a promising PS for PDT. Unfortunately, though the cell survival percent decreased gradually with the drug concentration increasing, the cell survival percentage of ArgZnPc treated cells is still as high as 89% after irradiation for 5 min (**Figure 13**), which indicates ArgZnPc may be not an efficient PS for PDT. The poor *in vitro* photocytotoxicity of ArgZnPc is also in line with its poor $^1\text{O}_2$ and intracellular ROSs generation ability and low cellular uptake efficiency.

3. Conclusion

In summary, we have studied the charge properties, photobiological, photochemical properties and *in vitro* anticancer activities of two arginine substituted ZnPcs for PDT. Both ArgEZnPc and ArgZnPc are water soluble and positively charged in the pH range of 5-9 due to their guanidine groups. ArgEZnPc exhibits high $^1\text{O}_2$ and intracellular ROSs generation efficiency, as well as high cellular uptake, the values of which is as high as 96% after 24 h incubation. It also shows preferential localization in the lysosomes of the HeLa cells. Moreover, upon irradiation, it exhibits excellent cytotoxicity towards HeLa cells. Nearly 90% cancer cells were killed after treatment by ArgEZnPc and 5 min irradiation. However, ArgZnPc exhibits poor photochemical and *in vitro* anticancer activity though it is also positively charged in a wide pH range. This may be attributed to that the guanidine and carboxyl groups of it can form inner salts, which weakens its activity. All these results show that the arginine substituted ArgEZnPc is highly promising PS for PDT.

4. Experimental Section

4.1. Materials and characteristics

All solvents and reagents were of reagent grade and used as received unless otherwise stated. The two arginine substituted zinc Pcs **ArgZnPc** and **ArgEZnPc** were prepared according to the article [32].

Zeta potential and DLS were taken on Zetasizer Nano ZS90, Malvern. UV-Vis and fluorescence spectra were measured on Cary 5000 spectrophotometer and Cary Eclipse Fluorescence spectrophotometer, respectively. Cell morphology and fluorescence inside the cells were monitored on a Nikon Ti Fluorescence microscope. Subcellular location studies were measured on BIORAD MRC-1024 confocal laser scanning microscope. A 665 nm LED (power density was 96 mW cm^{-2}) lamp was used as light source. Illumination of 5 min led to a

totally fluence of 28.8 J cm⁻².

4.2. Zeta potential measurement

Zeta potentials were measured in solutions of different pH values (5-9) at room temperature. The values represented mean \pm standard deviation (SD) of three separate experiments. It should note that since the zeta potential is related to salts concentration, the pH of the solutions was adjusted by NaOH (0.1%) and HCl (0.1%) solutions rather than buffer solutions.

4.3. ¹O₂ detection

Disodium salt of 9, 10-anthracene dipropionic acid (ADPA) was used as the scavenger for the detection of ¹O₂. ADPA can be bleached by ¹O₂, which can be monitored spectrophotometrically by recording the absorbance intensity decrease at 378 nm. ZnPcs (5 μ M) and ADPA (ca. 5.5 μ M) were mixed and irradiated with a 665 nm LED light. The decrease of ADPA at 378 nm was monitored every 30 s. After then, the ¹O₂ generation ability of the Pcs were calculated by the equation [47]:

$$\ln(ADPA_t/ADPA_o)=kt$$

Where $ADPA_o$ and $ADPA_t$ are the concentrations of ADPA before and after irradiation, respectively, t is the irradiation time, k is the ¹O₂ generation ability.

4.4. Cell lines and culture conditions

The HeLa cells were maintained in Dulbecco's modified Eagle's medium (DMEM) supplemented with fetal bovine serum (10%, v/v), streptomycin (0.1 mg·mL⁻¹), sodium pyruvate (110 mg·L⁻¹), L-glutamine (2 mM) and pyridoxine hydrochloride. Approximately 1 \times 10⁵ cells per well in the media were inoculated in 96-well plates and incubated in a moisturized atmosphere maintained at 37 °C in a 5.0% CO₂ atmosphere.

4.5. Intracellular ROSs detection

Intracellular ROSs generation of ArgZnPc and ArgEZnPc was measured by using 2',7'-dichlorofluorescein diacetate (DCFH-DA) as the probe. DCFH-DA did not have fluorescence in solution, while its oxidized form 2',7'-dichlorofluorescein (DCF) was highly fluorescent [48,49]. The intracellular ROSs production can be evaluated by recording the change of intracellular fluorescence intensity. HeLa cells were seeded on 6-well cell culture plates at a density of 1 \times 10⁵ cells per well. After incubation with the ZnPcs (4 μ M) for 24 h, cells were incubated with DCFH-DA (10 μ M). 30 min later, the cells were washed with phosphatebuffered saline (PBS) three times and irradiated with 665 nm LED for 5 min. After then, fluorescence of DCF was detected using an inverted fluorescence microscope (Ex= 488 nm; Em=530 nm).

4.6. Cellular uptake

Time dependent cellular uptake efficiency of **ArgZnPc** and **ArgEZnPc** were investigated as follows. HeLa cells with **ArgZnPc** and **ArgEZnPc** were incubated under the same experimental conditions as mentioned above for certain time (2 h, 4 h, 6 h, 24 h) in the dark. After then, the upper drug-containing medium was transferred in a 1 cm cuvette to measure the absorption spectra. The cellular uptake amounts were calculated according to the standard curves.

4.7. Cell morphology and Hoechst 33342 staining (nuclear morphology).

HeLa cells at adensity of 1×10^5 cells per well were seeded on 6-well plates. After 24 h incubation, the cells were rinsed with PBS, and then incubated with **ArgZnPc** and **ArgEZnPc** for another 4 h. Then, the cells were irradiated with 665 nm LED for 5 min and incubated for another 24 h. The cell morphology changes were observed under a fluorescence microscope.

Like the cell morphology measurement procedure, after washing by PBS, the HeLa cells were further treated with $5 \text{ mg} \cdot \text{mL}^{-1}$ Hoechst 33342 for 30 min in dark. The nuclear morphology changes were also measured under a fluorescence microscope.

4.8. Subcellular location studies

HeLa cells were seeded on a cell culture plate at adensity of 1×10^5 cells per well. After treatment with the solutions of **ArgZnPc** and **ArgEZnPc** ($4 \mu\text{M}$) for 12 h, the lysosomal tracker (Lyso Tracker Green DND-26, $2 \mu\text{M}$) or nuclear tracker (Hoechst 33342, $2 \mu\text{M}$) was then added and the cells were incubated for another 20 min. The cells were then washed with PBS three times and viewed with confocal laser scanning microscope. **ArgZnPc** and **ArgEZnPc** were excited at 633 nm and monitored at 650-750 nm. Lyso-Tracker was excited at 488 nm and monitored at 510-570 nm, while Nu-Tracker was excited at 351 nm and monitored at 410-500 nm. The subcellular localization of **ArgZnPc** and **ArgEZnPc** were revealed by comparing the intracellular fluorescence images caused by the Trackers and the dyes.

4.9. *In vitro* PDT studies with tumor cells

HeLa cells at adensity of 5×10^5 cells per well were seeded on 96-well plates. 24 h later, after being rinsed with PBS, HeLa cells were incubated with **ArgZnPc** and **ArgEZnPc** (0, 1, 2, 3, $4 \mu\text{M}$) for 4 h. After then, the cells were irradiated with 665 nm LED for 5 min. Then, the cells were placed back in the incubator for another 24 h. The cell viability was determined by means of the colorimetric MTT assay [46].

4.10. Statistical analysis

All the experimental results presented in this article are given as mean result \pm SD

(standard deviation). Differences between the values were assessed using Student's t-test and considered significant at the $P < 0.05$ level. The results used in the paper were from three independent experiments.

5. Acknowledgements

This work was supported by the National Nonprofit Institute Research Grant of CAFINT (CAFYBB2017SY031), the National Sci-Tech plan projects (2015BAD14B0601).

6. Figures

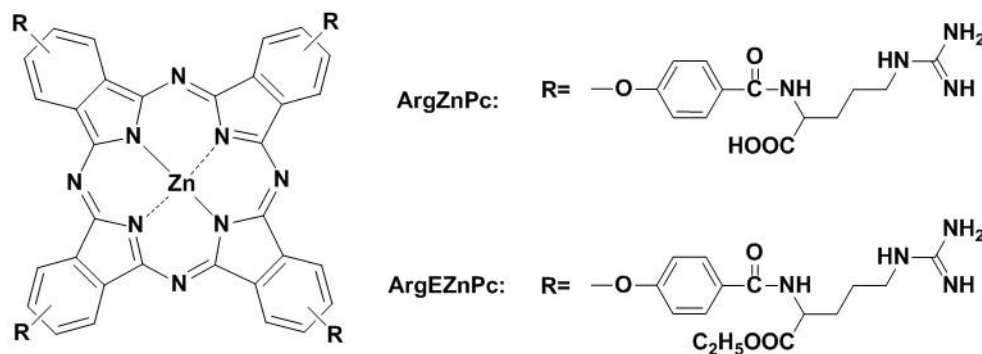


Figure 1: Structures of ArgEZnPc and ArgZnPc

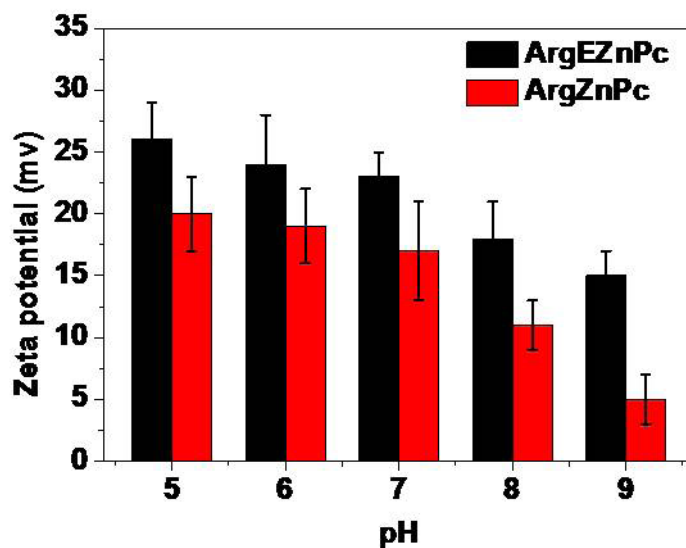


Figure 2: Zeta potentials of ArgZnPc and ArgEZnPc at different pH levels

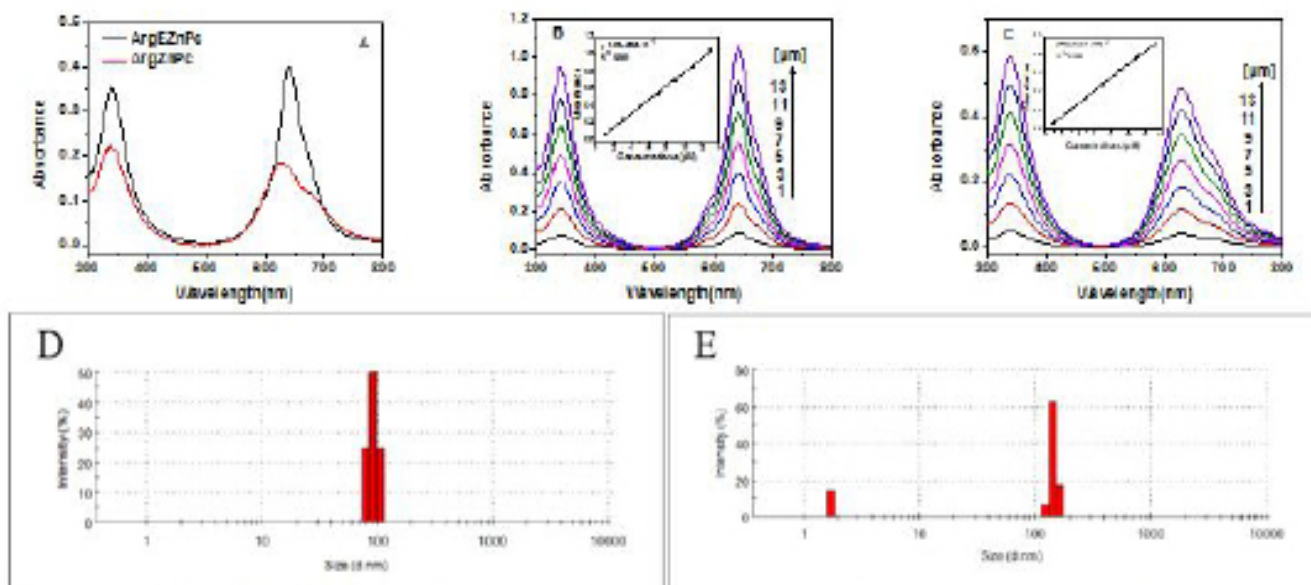


Figure 3: (A) Electronic absorption spectra of ArgEZnPc and ArgZnPc ($C=5 \times 10^{-6}$ M). UV-Vis spectra of ArgEZnPc (B) and ArgZnPc (C) at different concentrations (inset: plots the Q-band absorbance at 640 nm versus the concentration of ArgEZnPc and ArgZnPc). DLS analysis of ArgEZnPc (D) and ArgZnPc (E).

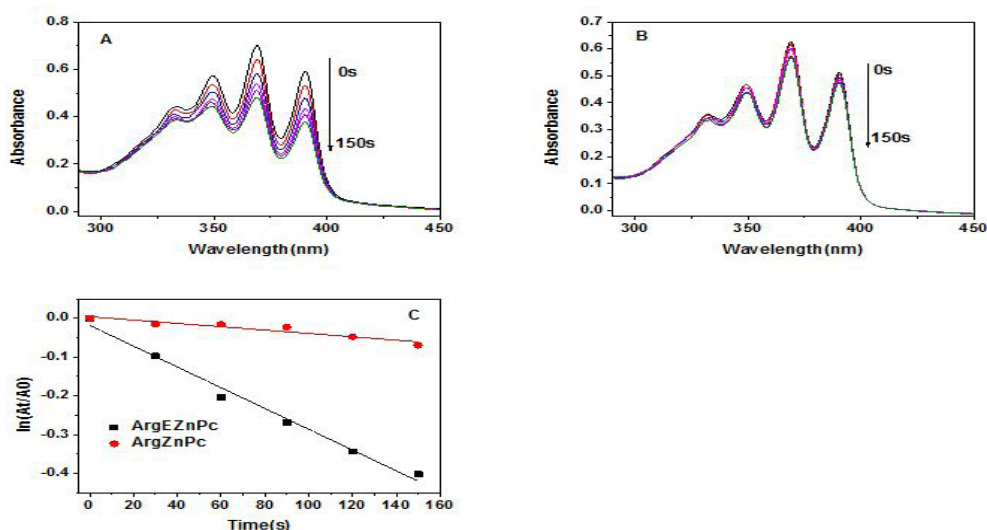


Figure 4: Time-dependent decrease of ADPA caused by 1O_2 generated by ArgEZnPc (A) and ArgZnPc (B) ($C=5 \times 10^{-6}$ M) upon irradiation for 0 s, 30 s, 60 s, 90 s, 120 s, 150 s with 665 nm LED. (C) photodegradation rate constants of ArgEZnPc and ArgZnPc

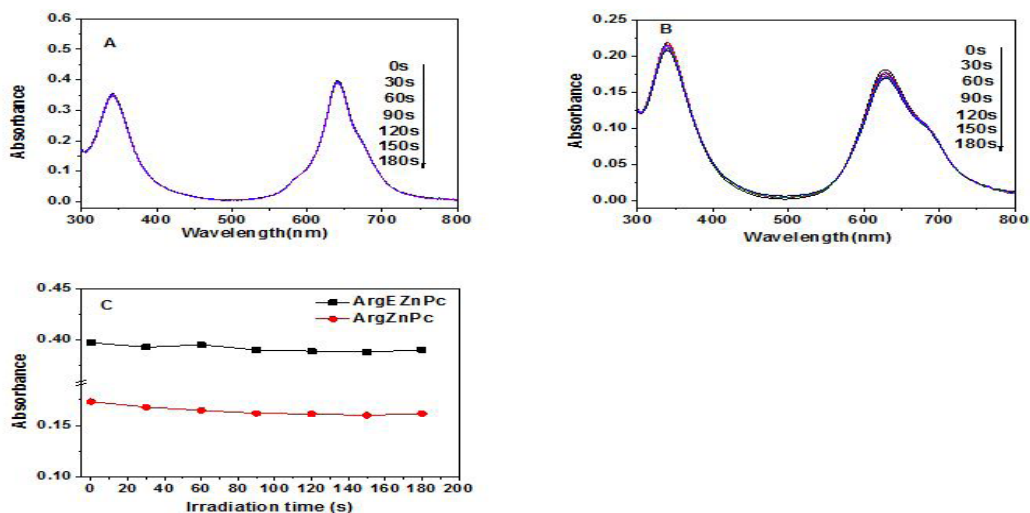


Figure 5: Time-dependent photobleaching of ArgEZnPc (A) and ArgZnPc (B) ($C=5 \times 10^{-6}$ M) upon irradiation for 0 s, 30 s, 60 s, 90 s, 120 s, 150 s, and 180 s with 665 nm LED light. (C) Q band change of ArgEZnPc and ArgZnPc versus irradiation time

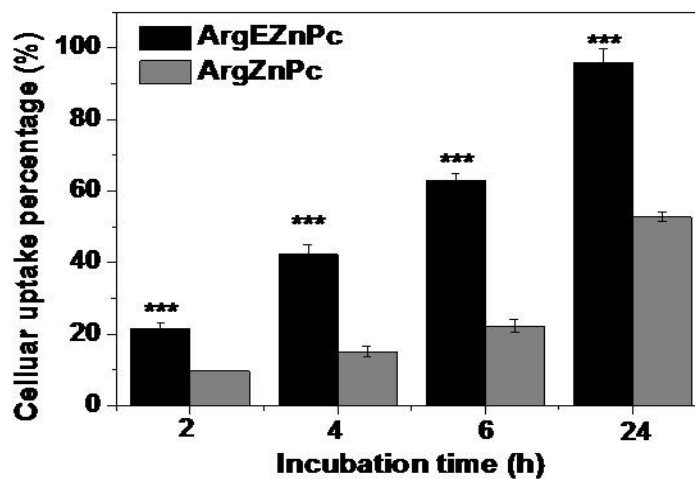


Figure 6: Cellular uptake of ArgEZnPc and ArgZnPc by HeLa cells versus incubation times (Data are expressed as means \pm SD; * P <0.05; ** P <0.01; *** P <0.001, ArgEZnPc vs. ArgZnPc)

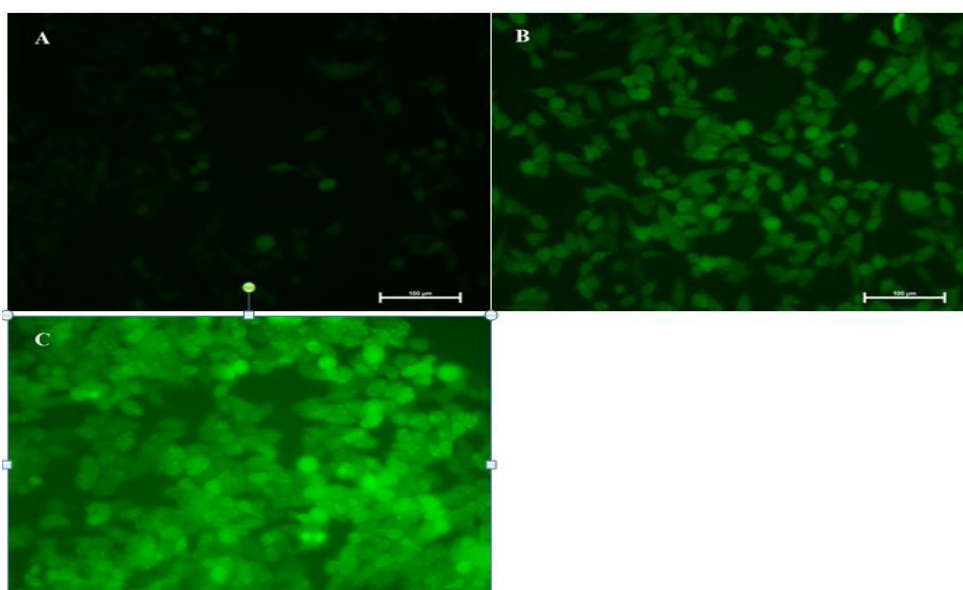


Figure 7: Visualization of the intracellular fluorescence of HeLa cells after treatment by (A) control, without drugs (B) ArgZnPc (C) ArgEZnPc and irradiation using DCFH-DA as the probe (Bar=100 μ M)

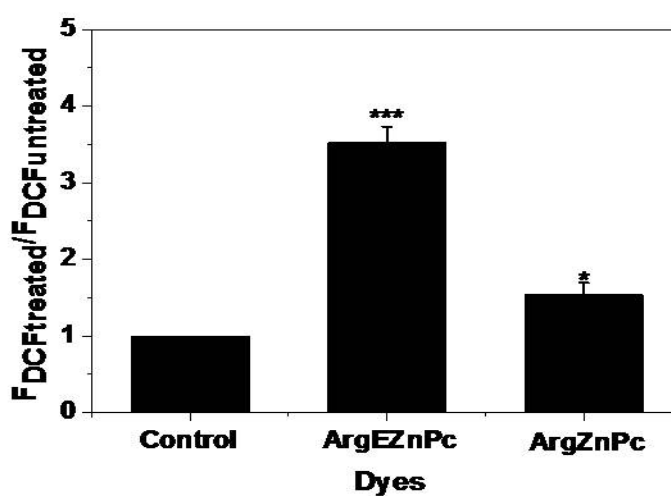


Figure 8: Effects of ArgEZnPc and ArgZnPc on intracellular ROSs generation (Data are expressed as means \pm SD; * P <0.05, *** P <0.001 vs. control; control means that cells were treated without Pcs)

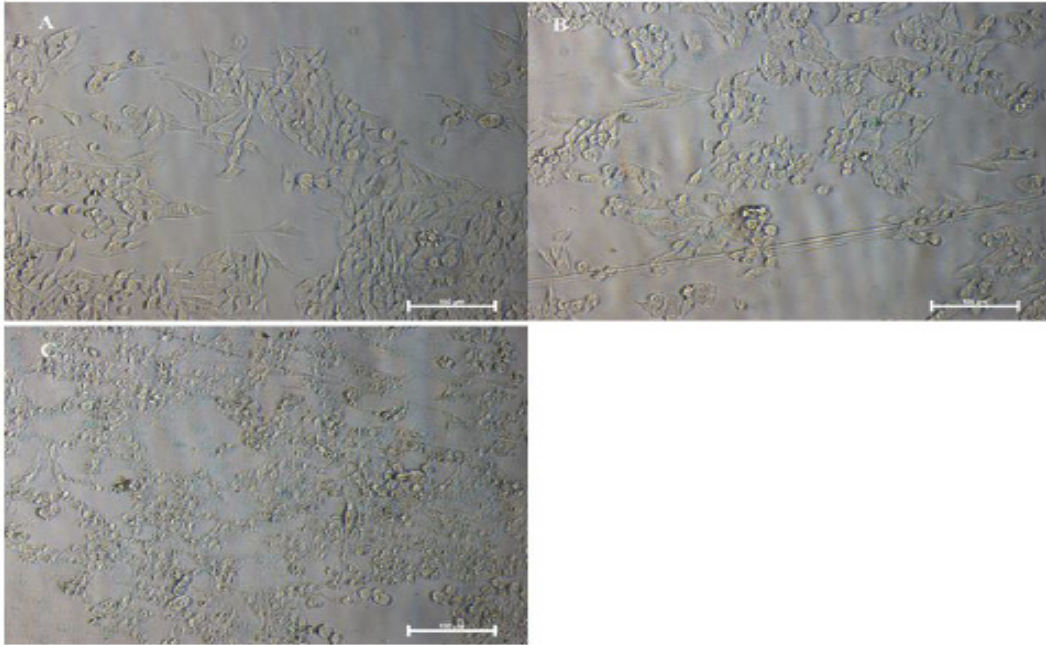


Figure 9: Morphology of HeLa cells treated with/without drugs and irradiated with 665 nm light (A) control, without drugs (B) ArgZnPc (C) ArgEZnPc ($C=5 \times 10^{-6}$ M; Bar= $100 \mu\text{m}$)

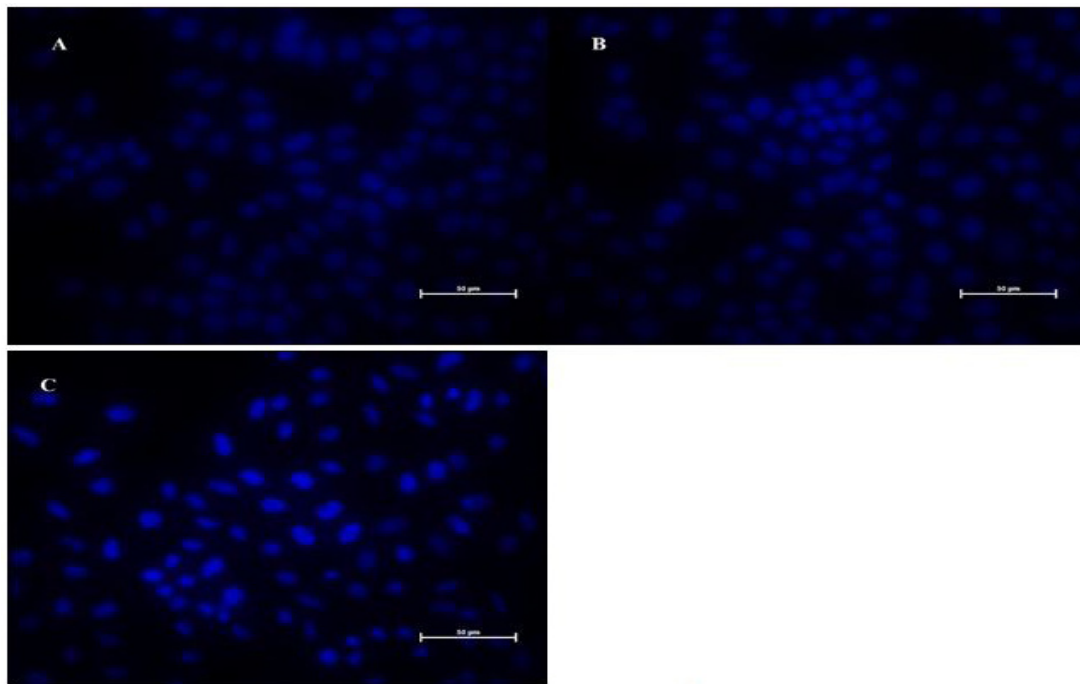


Figure 10: Nuclear morphology of HeLa cells treated with/without drugs and irradiated with 665 nm light (A) without drugs, control (B) ArgZnPc (C) ArgEZnPc ($C=5 \times 10^{-6}$ M; Bar= $50 \mu\text{m}$)

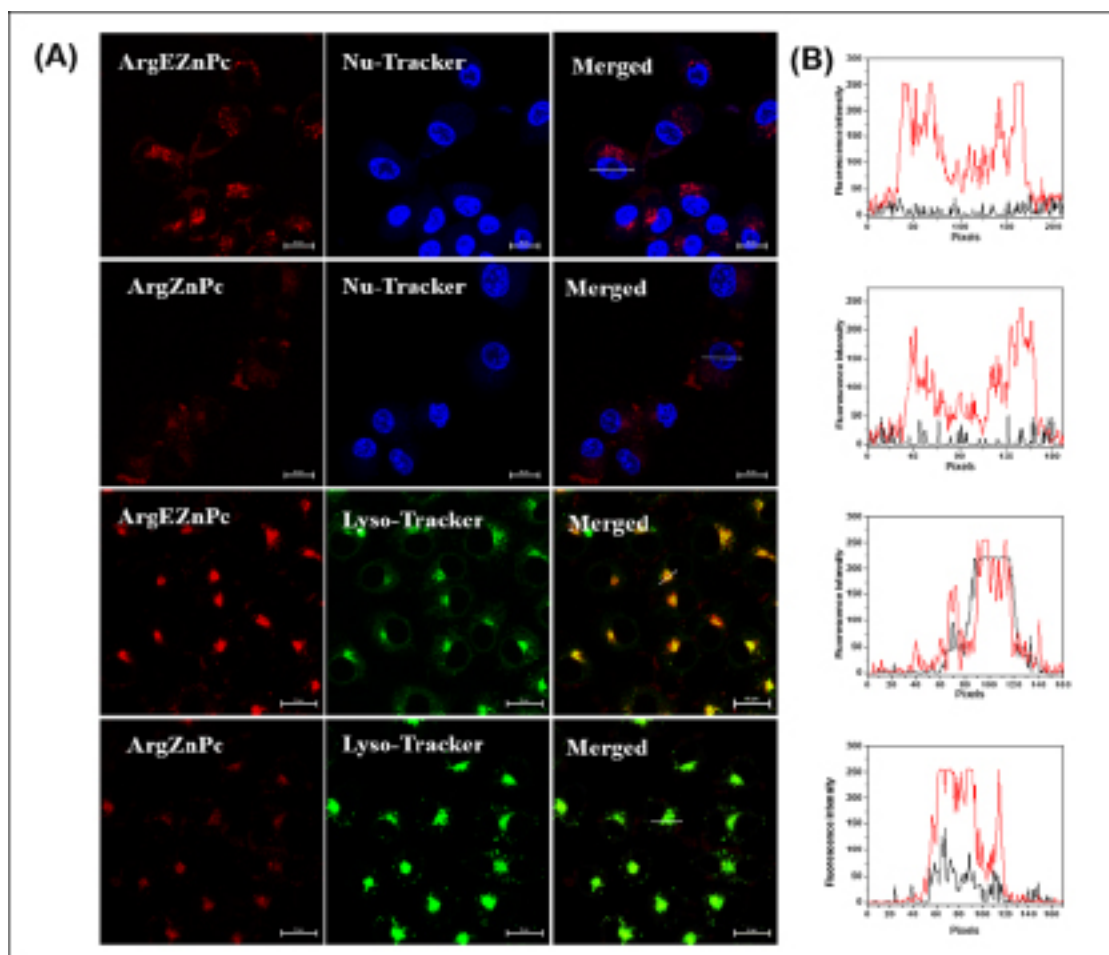


Figure 11: (A) Visualization of intracellular fluorescence of HeLa cells using filter sets specific for ArgZnPc and ArgEZnPc (in red), Nu-Tracker (in blue), Lyso-Tracker (in green) and the corresponding superimposed image. (B) in situ fluorescence analysis of merged images trace along the white arrow.

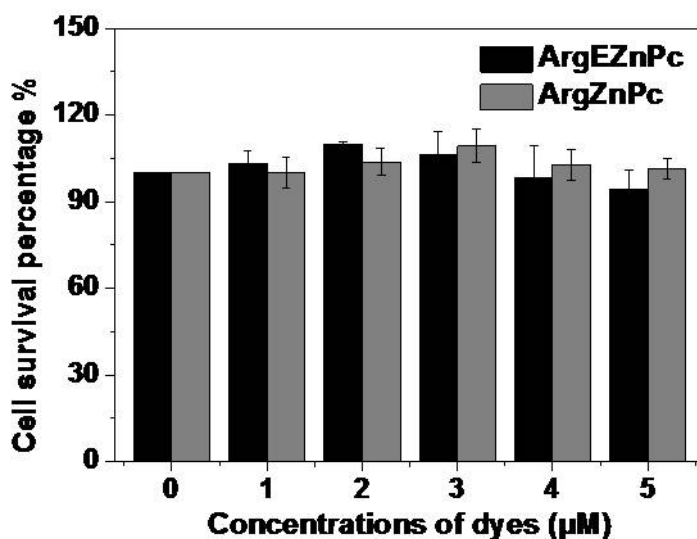


Figure 12: Concentration-dependent cytotoxicity of ArgEZnPc and ArgZnPc in the absence of light (Data are expressed as means \pm SD)

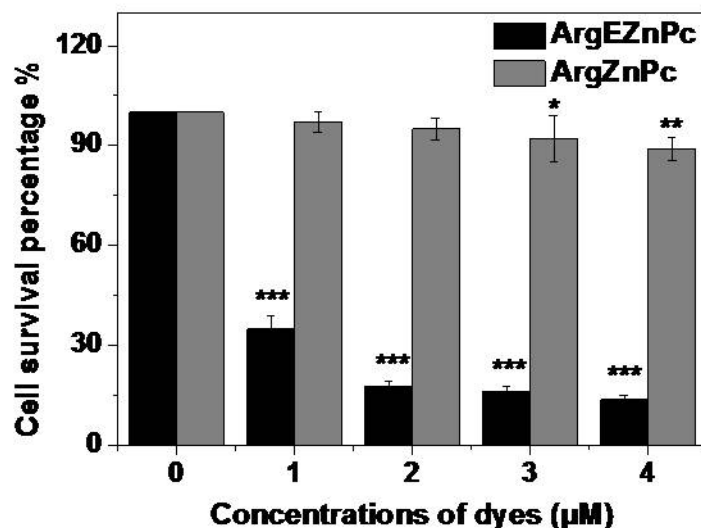


Figure 13: Concentration-dependent cytotoxicity of ArgEZnPc and ArgZnPc in the presence of light (Data are expressed as means \pm SD; * $P < 0.05$, ** $P < 0.01$, *** $P < 0.001$ vs. control)

7. References

1. Abdel-Kader, M. H. Photodynamic therapy: from theory to application, Springer Science & Business Media: Berlin, 2014.
2. Agostinis, P. Berg, K. Cengel, K. A. Foster, T. H. Girotti, A. W.; Gollnick, S. O.; Hahn, S. M.; Hamblin, M. R.; Juzeniene, A.; Kessel, D.; Korbelik, M.; Moan, J.; Mroz, P.; Nowis, D.; Piette, J.; Wilson, B. C.; Golab, J. CA-Cancer J. Clin. 2011, 61, 250.
3. You, H.; Yoon, H. E.; Jeong, P. H.; Ko, H.; Yoon, J. H.; Kim, Y. C. Bioorg. Med. Chem. 2015, 23, 1453.
4. Shi, G.; Monro, S.; Hennigar, R.; Colpitts, J.; Fong, J.; Kasimova, K.; Yin, H.; DeCoste, R.; Spencer, C.; Chamberlain, L.; Mandel, A.; Lilge, L.; McFarland, S. A. Coord. Chem. Rev. 2015, 283, 127.
5. Awuah, S. G.; You, Y. RSC Adv. 2012, 2, 11169.
6. Lamch, L.; Kulbacka, J.; Pietkiewicz, J.; Rossowska, J.; Dubinska-Magiera, M.; Choromanska, A.; Wilk, K. A. J. Photochem. Photobiol. B 2016, 160, 185.
7. Jiang, X. J.; Lo, P. C.; Tsang, Y. M.; Yeung, S. L.; Fong, W. P.; Ng, D. K. P. Chem. Eur. J. 2010, 16, 4777.
8. Li, J.; Zhang, X.; Liu, Y.; Yoon, I.; Kim, D. K.; Yin, J. G.; Wang, J. J.; Shim, Y. K. Bioorg. Med. Chem. 2015, 23, 1684.
9. Agarwal, R.; Roy, K. Ther. Delivery 2013, 4, 705.
10. Kryman, M. W.; Davies, K. S.; Linder, M. K.; Ohulchanskyy, T. Y.; Detty, M. R. Bioorg. Med. Chem. 2015, 23, 4501.
11. Wang, A.; Li, Y.; Zhou, L.; Yuan, L.; Lu, S.; Lin, Y.; Zhou, J.; Wei, S. J. Photochem. Photobiol. B 2014, 141, 10.
12. Opanasopit, P.; Rojanarata, T.; Apirakaramwong, A.; Ngawhirunpat, T.; Ruktanonchai, U. Int. J. Pharm. 2009, 382, 291.
13. Makhseed, S.; Machacek, M.; Alfadly, W.; Tuhl, A.; Vinodh, M.; Simunek, T.; Novakova, V.; Kubat, P.; Rudolfe, E.; Zimcik, P. Chem. Commun. 2013, 49, 11149.
14. Machacek, M.; Cidlina, A.; Novakova, V.; Svec, J.; Rudolf, E.; Miletin, M.; Kucera, R.; Simunek, T.; Zimcik, P. J. Med. Chem. 2015, 58, 1736.

15. Li, X. S.; Guo, J.; Zhuang, J. J.; Zheng, B. Y.; Ke, M. R.; Huang, J. D. *Bioorg. Med. Chem. Lett.* 2015, 25, 2386.
16. Tian, J.; Ding, L.; Xu, H. J.; Shen, Z.; Ju, H.; Jia, L.; Bao, L.; Yu, J. S. *J. Am. Chem. Soc.* 2013, 135, 18850.
17. McDonnell, S. O.; Hall, M. J.; Allen, L. T.; Byrne, A.; Gallagher, W. M.; O'Shea, D. F. *J. Am. Chem. Soc.* 2005, 127, 16360.
18. Wang, A.; Ma, Y.; Zhou, L.; Lu, S.; Lin, Y.; Zhou, J.; Wei, S. *Dyes Pigm.* 2013, 99, 348.
19. Dumoulin, F.; Durmus, M.; Ahsen, V.; Nyokong, T. *Coord. Chem. Rev.* 2010, 254, 2792.
20. Luedtke, N. W.; Baker, T. J.; Goodman, M.; Tor, Y. J. *J. Am. Chem. Soc.* 2000, 122, 12035.
21. Bergeron, R. J.; McManis, J. S.; Weimar, W. R.; Schreier, K. M.; Gao, F.; Wu, Q.; Ortiz-Ocasio, J.; Luchetta, G. R.; Porter, C.; Vinsont, J. R. *J. Med. Chem.* 1995, 38, 2278.
22. Yang, F.; Xia, X.; Lei, H. Y.; Wang, E. D. *J. Biol. Chem.* 2010, 285, 39437.
23. Fu, X.; Tan, C. H. *Chem. Commun.* 2011, 47, 8210.
24. Gobbi, A.; Frenking, G. J. *J. Am. Chem. Soc.* 1993, 115, 2362.
25. Echavarren, A.; Galan, A.; Lehn, J. M.; Mendoza, J. D. *J. Am. Chem. Soc.* 1989, 111, 4994.
26. Yaku, H.; Fujimoto, T.; Murashima, T.; Miyoshi, D.; Sugimoto, N. *Chem. Commun.* 2012, 48, 6203.
27. Alzeer, J.; Vummidi, B. R.; Roth, P. J. C.; Luedtke, N. W. *Angew. Chem. Int. Ed.* 2009, 48, 9362.
28. Luedtke, N. W.; Carmichael, P.; Tor, Y. J. *J. Am. Chem. Soc.* 2003, 125, 12374.
29. Raczynska, E. D.; Cyranski, M. K.; Gutowski, M.; Rak, J.; Gal, J. F.; Maria, P. C.; Darowska, M.; Duczmal, K. *J. Phys. Org. Chem.* 2003, 16, 91.
30. Singh, S.; Aggarwal, A.; Bhupathiraju, N. V. S. D. K.; Arianna, G.; Tiwari, K.; Drain, C. M. *Chem. Rev.* 2015, 115, 10261.
31. Garcia, A. M.; Weerasekera, H. A.; Pitre, S. P.; McNeill, B.; Lissi, E.; Edwards, A. M.; Alarcon, E. I. *J. Photochem. Photobiol. B* 2016, 163, 385.
32. Wang, A.; Zhou, R.; Zhou, L.; Sun, K.; Zhou, J.; Wei, S.; Jiang, J. *Chem. Asian J.* 2016, 11, 3008.
33. Yanik, H.; Al-Raqa, S. Y.; Aljuhani, A.; Durmus, M. *Dyes Pigm.* 2016, 134, 531.
34. Wang, A.; Jin, W.; Chen, E.; Zhou, J.; Zhou, L.; Wei, S. *Dalton Trans.* 2016, 45, 3853.
35. Zhai, D.; Xu, W.; Zhang, L.; Chang, Y. T. *Chem. Soc. Rev.* 2014, 43, 2402.
36. Sitaram, N.; Nagaraj, R. *BBA-Biomembranes* 1999, 1462, 29.
37. Nyokong, T. *Coord. Chem. Rev.* 2007, 251, 1707.
38. Du, J. Z.; Sun, T. M.; Song, W. J.; Wu, J.; Wang, J. *Angew. Chem. Int. Ed.* 2010, 49, 3621.
39. Vummidi, B. R.; Noreen, F.; Alzeer, J.; Moelling, K.; Luedtke, N. W. *ACS Chem. Biol.* 2013, 8, 1737.
40. Perttu, E. K.; Jr, F. C. S. *Chem. Commun.* 2011, 47, 12613.
41. Zheng, Y. J.; Ornstein, R. L. *J. Am. Chem. Soc.* 1996, 118, 11237.

42. Zhou, L.; Jiang, H.; Wei, S.; Ge, X.; Zhou, J.; Shen, J. *Carbon* 2012, 50, 5594.
43. Lucky, S. S.; Soo, K. C.; Zhang, Y. *Chem. Rev.* 2015, 115, 1990.
44. Tachikawa, S.; Sato, S.; Hazama, H.; Kaneda, Y.; Awazu, K.; Nakamura, H. *Bioorg. Med. Chem.* 2015, 23, 7578.
45. Rajaputra, P.; Nkepan, G.; Watley, R.; You, Y. *Bioorg. Med. Chem.* 2013, 21, 379.
46. Jiang, X. J.; Yeung, S. L.; Lo, P. C.; Fong, W. P.; Ng, D. K. P. *J. Med. Chem.* 2011, 54, 320.
47. Tang, W.; Xu, H.; Kopelman, R.; Philbert, M. A. *Photochem. Photobiol.* 2005, 81, 242.
48. Garcia, D. H.; Wood, C. D.; Obregon, S. C.; Covarrubias, L. *Free Radical Bio. Med.* 2010, 49, 130.
49. Gomes, A.; Fernandes, E.; Lima, J. L. F. C. *J. Biochem. Biophys. Methods* 2005, 65, 45.